APPLIED GEOPHYSICS, Vol.21, No.4 (December 2024), P. 1−11, 9 Figures.
DOI:10.1007/s11770-024-1106-7

Three-dimensional geothermal reservoir model using the magnetotelluric method in medium and deep strata of Yishu fault zone, Rizhao Section

Du Wenlong[1], Zhou Xingyu[1]*, Sun Yuanbin[1], Wang Shidang[1], Zhang Dabin[1], Wang Chen[1], Zhang Jinwei[2], and Ding Renwei[2]

Abstract: The Yishu fault zone in Shandong Province, China, exhibits favorable conditions for medium- and high-temperature geothermal storage. However, its geothermal occurrence patterns and heat storage model remain unclear. Recognizing the importance of deep heat sources and heat channels in unraveling the formation mechanisms of medium- and high-temperature geothermal systems, we conducted a magnetotelluric survey along the Yishu fault zone, which contained 10 survey lines and 119 usable points. Using two-dimensional and three-dimensional nonlinear conjugate gradient inversion, the deep electrical structure was obtained, and the three-dimensional geothermal reservoir model in the study area was constructed for the first time. The results show that the deep low-resistance anomaly in the Yishu fault zone moves upward through the channel with slightly higher resistivity, forming a relatively low-resistance layer and a low-resistance layer in the shallow part, corresponding to the heat source, thermal conduction fault, heat reservoir, and overburden layer, respectively. The fault structure primarily controls regional geothermal anomalies, influencing atmospheric precipitation, surface water infiltration, and geothermal water migration pathways. The results of this study have a certain guiding significance for the study of the formation mechanism and distribution law of geothermal resources in the middle and deep strata of the Yishu fault zone. Additionally, the results provide valuable insights for the exploration and assessment of geothermal resources in the area.
Keywords: Yishu fault zone; magnetotelluric sounding; geothermal model; heat flow channel

Introduction

Geothermal energy is a type of renewable green energy, and its development and utilization are of great significance for China to realize carbon peaking and carbon neutrality goals (Agemar, 2022). Geothermal resources in Shandong Province are abundant and widely distributed, offering immense potential for development and utilization.

The spatial distribution of heat flow in Shandong Province is closely related to its tectonic patterns (Figure 1). On the basis of the comprehensive analysis of its geothermal genesis and heat storage types, the province can be further divided into four geothermal resource areas: I. Ludong geothermal area; II. Yishu fault zone geothermal area; III. Luxi Uplift geothermal area; and IV. Northwest Shandong geothermal area. The Luxi Uplift geothermal area can be further subdivided into the Luzhong Uplift geothermal subarea and the Southwest

Manuscript received by the Editor March 28, 2024; revised manuscript received May 09, 2024.
This work was supported by LUMEIDIKE202326 .
1.The Third Exploration Team, Shandong Bureau of Coal Geology, Taian, 271000
2.College of Earth Science and Technology, Shandong University of Science and Technology, Qingdao, 266590
*Corresponding author: Zhou Xingyu, zhouxingyu2006@126.com.

Shandong Submarine Uplift geothermal subarea. The geothermal resources in the Ludong geothermal area, the Yishu fault zone geothermal area, and the geothermal subarea of the central Shandong uplift are characterized as convective geothermal resources associated with uplifted mountains. Conversely, the geothermal resources in the Northwest Shandong and Southwest Shandong geothermal subareas are classified as sedimentary basin conduction type.

The study area is located in the Yishu fault zone, which is characterized as a Moho surface uplift zone with a geothermal heat flow value of 62 mW/m². Previous studies (Deng et al., 2021; Liao et al., 2023; Liu et al., 2023; Yang et al., 2020) and geothermal surveys have provided initial insights into the geological background conditions of the geothermal area and identified the presence of geothermal anomalies within the Yishu fault zone. The properties and scale of heat control and water-conducting structures have been identified, laying the foundation for the exploration and rational development of geothermal resources in the region. However, the accuracy of geothermal geological research in the survey area remains relatively low. The insufficient availability of effective basic data and limited systematic research on the relationship between the Yishu fault zone (Rizhao section) and geothermal heating have hindered the determination of primary heat control mechanisms and geothermal storage models. The distribution of regional geothermal fields and geothermal anomaly areas is yet to be fully understood, leading to uncertain prospects for the development and utilization of these anomalous areas.

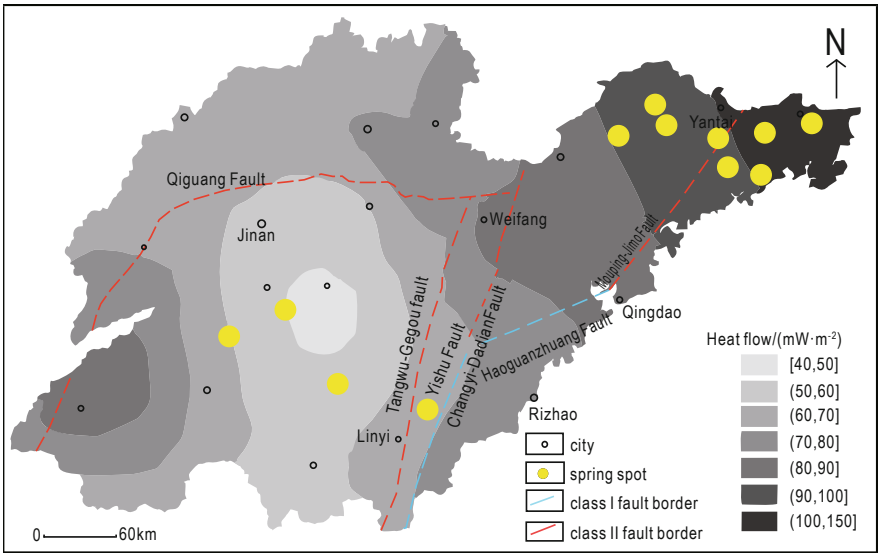

Figure 1. Terrestrial heat flux districts in Shandong Province (revised according to Liu et al. (2018)).

The magnetotelluric (MT) method is effective for studying the conductive structure and rheological characteristics of the Earth's interior (Vozoff, 1972), and it can provide an important basis for the study of deep-seated magmatic activity related to geothermal energy. The MT sounding method has a good resolution for deep-seated high conductors and can be used to explain the bottom intrusion of deep-seated basaltic magma related to geothermal energy (Kun et al., 2020) and the hydration process of the lithosphere caused by plate subduction (Li et al., 2022). It can also be used to study the deep-seated heat source mechanism of geothermal systems (Patro, 2017; Maithya and Fujimitsu, 2019) and the geological structures of unconventional geothermal reservoirs, among others (Lee et al., 2018; Chen et al., 2021; Liao et al., 2023; Mekkawi et al., 2022).

Based on previous studies, this paper analyzes the deep electrical structure and geothermal characteristics of the Yishu fault zone (Rizhao section) using the MT method. There are 10 survey lines and 119 usable survey points. The formation mechanism of deep geothermal resources and their distribution law are analyzed, which lays the foundation for the development and utilization of geothermal resources.

Geological background

The study area is at the north–central part of the

Jiaonan uplift and the southwest margin of the Jiaolai Basin (Figure 2). From bottom to top, the outcropping strata can be divided into the Paleoproterozoic Fanzishan Group, Mesozoic Cretaceous Laiyang Group, Qingshan Group, Dasheng Group, Wangshi Group, Cenozoic Quaternary Pleistocene, and Holocene sediments.

The Yishu fault zone, extending in the NNE direction throughout the whole of Shandong Province, is a highly intricate tectonic belt. It encompasses four major faults: the Yanyu–Gegou fault, the Yishui–Tangtou fault, the Anqiu–Juxian fault, and the Changyi–Dadian fault. These faults all cut through the crust and extend deep into the upper mantle (the depth of the Moho surface is about 30–50Km). These four main faults are categorized as crustal faults and form the tectonic pattern of "two graben and one horst." Moreover, numerous secondary faults branch out from each main fault, and these fault zones play a significant role in the emplacement and eruption of magma, particularly in relation to basic and ultrabasic rocks, as well as deep-seated xenoliths. The region exhibits a wide variety of magmatic rocks, primarily including latent volcanic rocks and Ludong intrusive rocks from the Sibao, Jinning, Nanhua, Indosinian, and Late Yanshan periods.

The frequent magmatic activity during the Mesozoic Yanshan period in this area connected the heat source in the deep crust. At and near the intersection of structures, deep structural fractures are developed, providing a good channel and storage place for deep water circulation. Hot water deep underground is prone to rise along fault channels, forming geothermal anomalies. Igneous rocks are widely distributed with strong neotectonic movements in the study area. Thus, the study area possesses geological and structural conditions for geothermal formation. Multiple hot springs and three geothermal wells have been discovered: the Tangtou geothermal well located between the Yanyi–Gegou fault and the Yishui–Tangtou fault, the Yinan Tongjing geothermal well on the west side of the Yanyi–Gegou fault, with a wellhead water temperature of 74°C, and the Wulian–Guanshuai geothermal well located on the Changyi–Dadian fault, with an effluent temperature of 56°C.

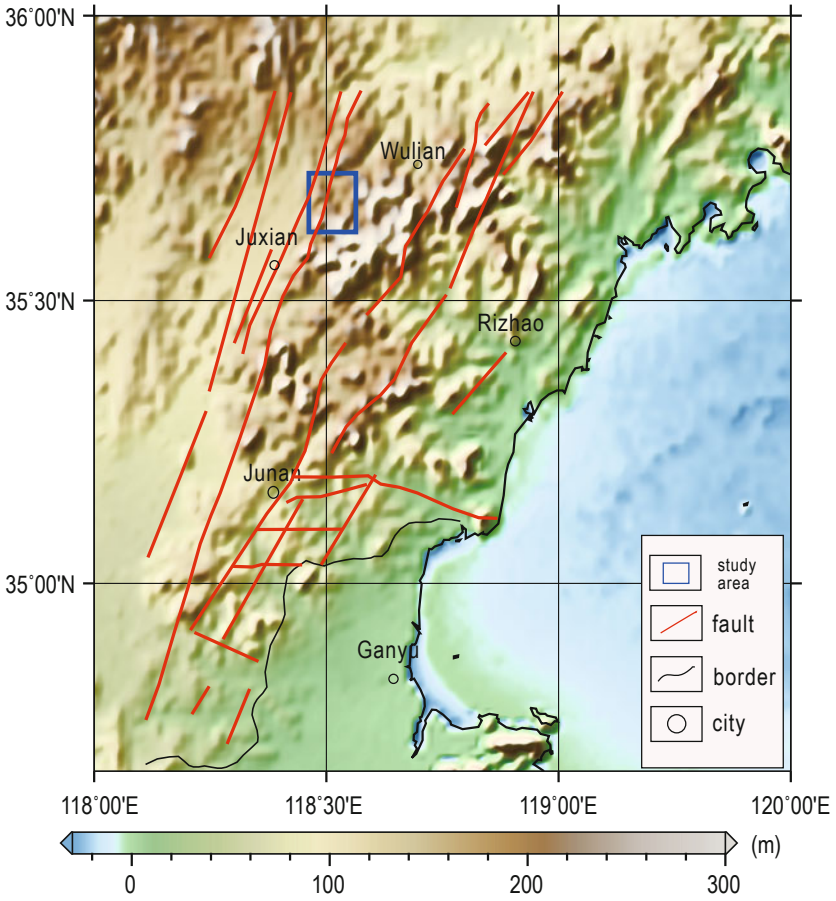

Figure. 2 Regional tectonic map and survey area.

Methodology and data

MT sounding

MT sounding is a passive exploration method used to map subsurface resistivity structures with the spatiotemporal variation of the natural electric field (E) and magnetic field (H) on the Earth's surface. Their sources mainly include lightning activity and the complex interaction between the solar wind and the Earth's magnetosphere and ionosphere. The far-field electromagnetic wave is approximately regarded as a plane electromagnetic wave perpendicular to the ground. By analyzing the characteristics of the electric and magnetic field components observed on the surface, the electrical structure of the subsurface can be explored (Ogawa and Junge, 2002; Dmitriev and Berdichevsky, 1979).

The MT method associates the horizontal electric field $\mathbf{E}_h$ with the horizontal magnetic field $\mathbf{H}_h$ using the concept of impedance tensor $\mathbf{Z}$ ($\mathbf{r}$, ω) as below:

$$\mathbf{E}_h(\mathbf{r},\omega) = \mathbf{Z}(\mathbf{r},\omega)\mathbf{H}_h(\mathbf{r},\omega)\,, \tag{1}$$

$$\mathbf{Z}(\mathbf{r},\omega) = \begin{bmatrix} Z_{xx}(\mathbf{r},\omega) & Z_{xy}(\mathbf{r},\omega) \\ Z_{yx}(\mathbf{r},\omega) & Z_{yy}(\mathbf{r},\omega) \end{bmatrix}, \tag{2}$$

$$\mathbf{E}_h(\mathbf{r},\omega) = \begin{bmatrix} E_x(\mathbf{r},\omega) \\ E_y(\mathbf{r},\omega) \end{bmatrix}, \tag{3}$$

$$\mathbf{H}_h(\mathbf{r},\omega) = \begin{bmatrix} H_x(\mathbf{r},\omega) \\ H_y(\mathbf{r},\omega) \end{bmatrix}, \tag{4}$$

where $\mathbf{r}$ represents the location of the observation spot, ω is the circular frequency, and x and y represent two mutually perpendicular horizontal directions. Then, we can use the impedance to express the apparent resistivity ρ* and phase ϕ:

$$\rho_{ij}^{*}(\mathbf{r},\omega) = \frac{1}{\omega\mu_0}\,|\,Z_{ij}(\mathbf{r},\omega)\,|^2\,, \tag{5}$$

$$\phi_{ij}(\mathbf{r},\omega) = \arctan\left[\frac{\mathrm{Im}\,Z_{ij}(\mathbf{r},\omega)}{\mathrm{Re}\,Z_{ij}(\mathbf{r},\omega)}\right], \tag{6}$$

where Im represents the imaginary part of the complex impedance and represents the real part. μ_0 is the magnetic conductivity in free space. With equations (5) and (6), we can have a preliminary knowledge of subsurface structures.

Nonlinear conjugate gradient (NLCG) inversion

The electrical conductivity structure of layered strata is obtained by inversion. There are many kinds of inversion methods, such as the Bostick transformation, rapid relaxation inversion, Occam inversion, conjugate gradient inversion, and so on. Among them, NLCG inversion is a fast, stable, and convergent inversion algorithm suitable for large-scale geophysical inversion problems (Rodi and Mackie, 2001; Newman and Alumbaugh, 2000).

The objective function used to solve the model is expressed as

$$O(\mathbf{m}) = \Delta d^T W^{-1}\Delta d + \lambda m^T L^T L m\,, \tag{7}$$

where $\Delta d = d - G(m)$ represents the misfit between observed and calculated data. $G(m)$ Is the forward modeling function, and W is the variance of the residual vector. λ is the regularization factor. L is a quadratic difference operator and approximates a Laplace operator when the grid is uniform.

Given the initial model m_0, the iterative process is mainly as follows:,

$$\begin{cases} O(m_k + \alpha_k p_k) = \min O(m_k + \alpha p_k), k = 0,1,2,\cdots \\ m_{k+1} = m_k + \alpha_k p_k \end{cases}, \tag{8}$$

where a_k is the step size and p_k is the search direction as

$$\begin{cases} p_0 = -C_0 g_0 \\ p_k = -C_k g_k + \beta_k p_{k-1} \end{cases}, \tag{9}$$

C_k is the preconditionality factor and g_k is the gradient at m_k. β_k is calculated using the Polak–Ribiere formula:

$$\beta_k = \frac{g_k^T C_k (g_k - g_{k-1})}{g_k^T C_k g_{k-1}}\,. \tag{10}$$

Data acquisition and processing

The V8 multifunctional networked electrical workstation produced by Phoenix Company of Canada was used for data acquisition. As shown in Figure 3, a total of 10 survey lines and 119 survey points were completed (only the survey points after selection are displayed in the figure). The point interval was about 1,000 m.

Other acquisition parameters include the following:

1) The electrodes were laid in the shape of a "+," and the distance of the potential electrode MN was 100 m.

2) The observation time was 8h. The apparent resistivity and phase curves were smooth and continuous (Figure 4). The apparent resistivity curves reveal noticeable variations in the electrical structure.

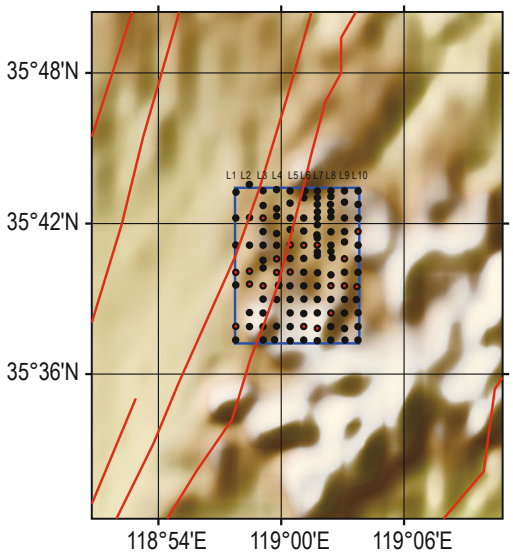

Figure 3. Survey line and survey points (red lines represent faults).

3) The acquisition frequency range was 320–0.00034Hz, including 80 frequencies, to ensure that the detection depth reached 8,000 m.

4) Robust impedance estimation and fixed station far-referential methods were adopted for the whole survey area to enhance data reliability and accuracy (Egbert, 1997; Ritter et al., 1998).

The field data of the MT method were the time series of electric field and magnetic field components. Only the data after preprocessing could be used for inversion and later interpretation (Kunetz, 1972; Travassos and Beamish, 1988). MT data preprocessing work mainly included spectrum analysis of electromagnetic field records in the time domain and robust processing, which transformed the data from the time domain to the frequency domain. As shown in Figure 4, the apparent resistivity at a short period (0.003–1 s) increased as the period increased, indicating that the shallow layer had a relatively high resistivity as caprocks. In the long period (1–1,000 s), the resistivity increased first and then decreased or decreased directly, indicating a low-resistance body corresponding to deep thermal storage. The low resistance in the deep might be the manifestation of the structure.

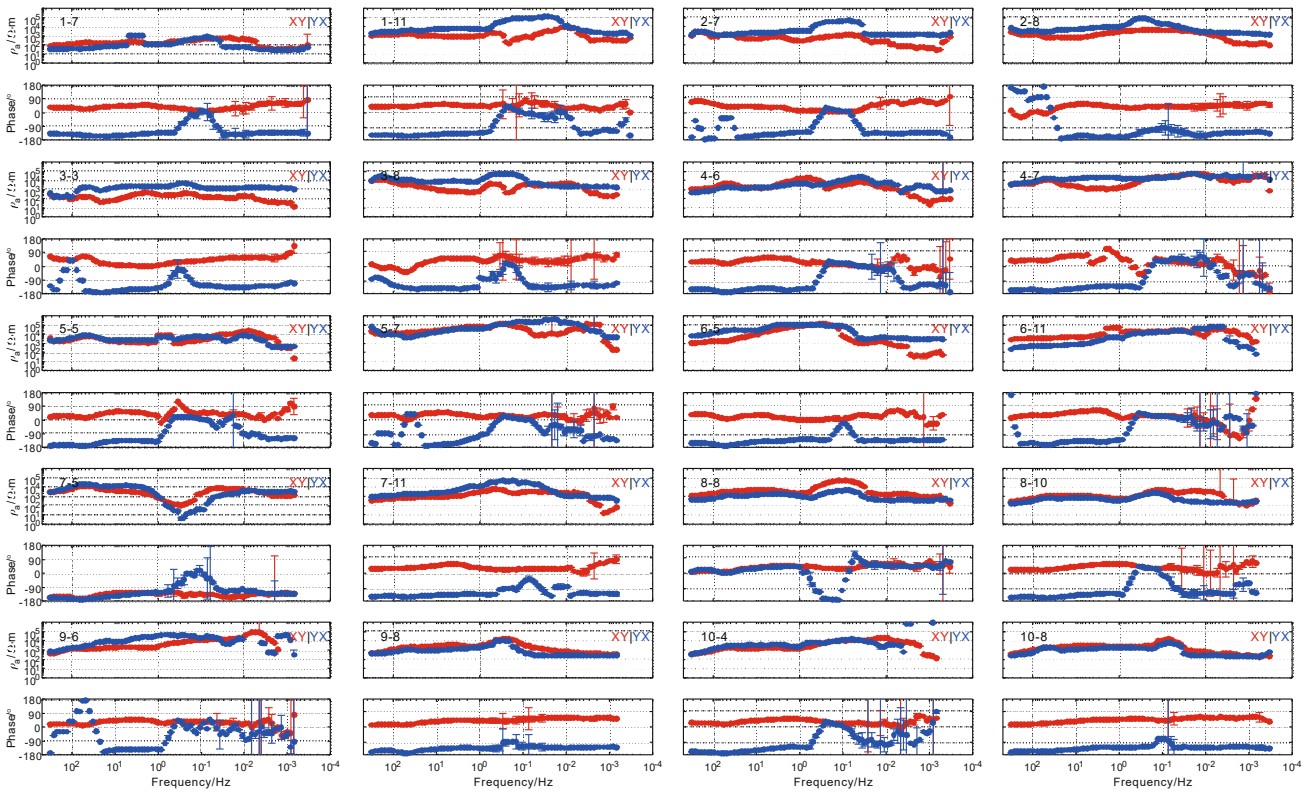

Figure 4. Apparent resistivity and phase curves of different measurement points (red points in Figure 3; first number for line and second number for point).

Afterward, the dimensional information and tectonic trends of subsurface electrical structure were analyzed as they were essential for inversion (Figure 5). In the shallow layers, most phase tensor ellipses were close to a perfect circle, and their skewness was small, reflecting that the shallow layer of the geothermal field was a Quaternary sediment with a near-one-dimensional resistivity structure. In the middle layers, the data had typical two-dimensional (2D) characteristics according to the G–B impedance tensor decomposition method (Groom and Bailey, 1989). In the middle and deep layers, the elliptical long axis was NE and NW, consistent with the strike of the main regional fault structures. In the deep subsurface (Figure 5d), the skewness of most survey points was greater than 5°, indicating a strong three-dimensional (3D) nature in the deep region. Therefore, a 3D inversion may yield more reliable information about the electrical structure in the deep subsurface.

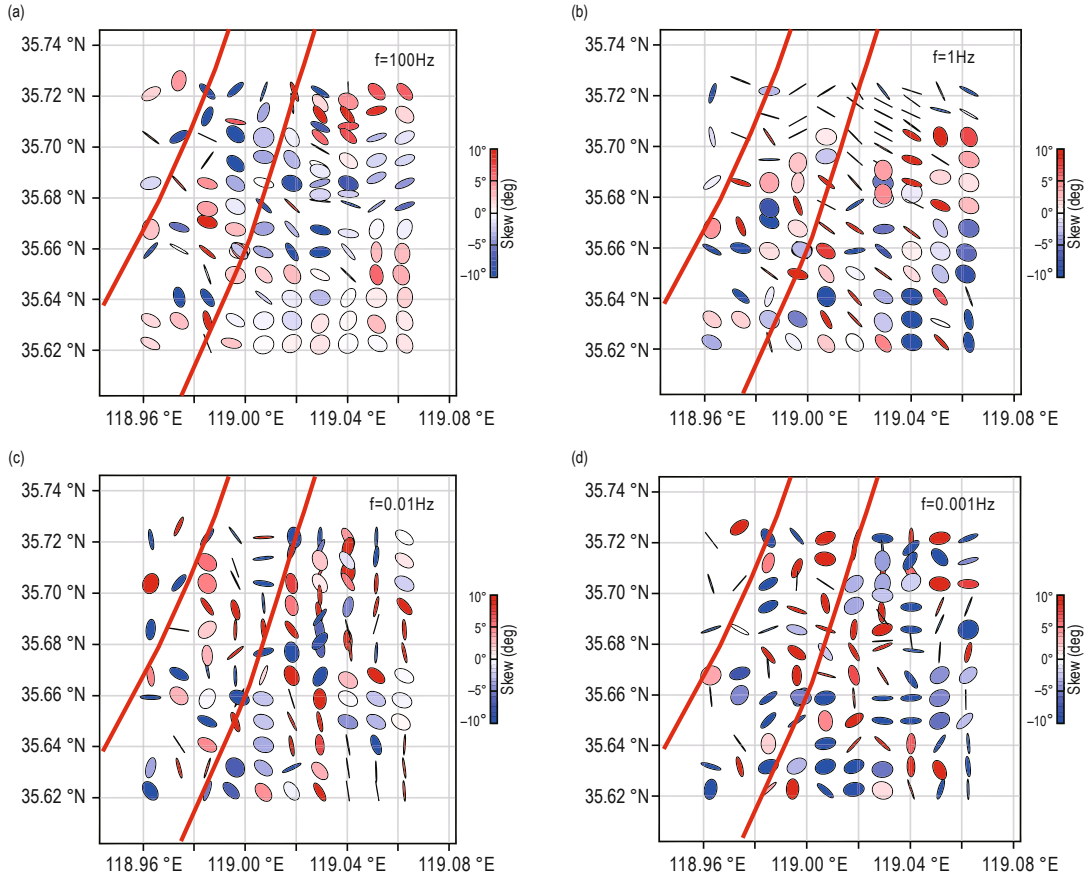

Figure 5. Phase tensor ellipsoids of different frequencies (the red lines represent faults).

Results and discussion

The 2D inversion modes for MT include TE, TM, and TE + TM modes. The TE mode is more sensitive to vertical resistivity variation, but the TE mode is more susceptible to 3D distortion (Berdichevsky and Weaver, 1999). Meanwhile, the TM mode has a good lateral resolution and insufficient vertical resolution. The TE + TM joint inversion model is often used in practice (Siripunvaraporn et al., 2005). In this paper, the TE + TM mode was used for the 2D inversion of data. After inversion tests containing different initial models, smoothness coefficients, and initial regularization factors, we obtained the optimal inversion results by setting the initial model with a uniform half-space of 1,000 Ω·m, a smoothness coefficient of 0.35, and an initial regularization factor of 6. Furthermore, a 3D inversion with ModEM (Egbert and Kelbert, 2012; Kelbert et al., 2014) was conducted to obtain a more comprehensive exhibition of the subsurface electric structure. The inversion residuals are shown in Figure 6.

Most measurement points had RMS values less than 2, and the level of single-point fitting error was close to the overall fitting error.

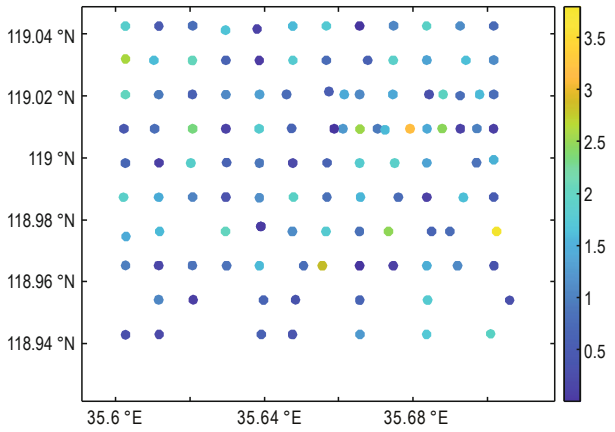

Figure 6. Statistics and distribution of residuals fitted to the inversion results.

According to the 2D and 3D inversion results, the subsurface resistivity characteristics were divided into two types: the shallow part with medium and low resistivity (below 500 Ω·m) was inferred as conglomerate, sandstone, shale, tuff, and andesite, among others, which acted as the caprock of the geothermal system. The resistivity below the caprock was significantly increased, which was presumed to be an electrical reaction of intrusive rocks and metamorphic rocks, that is, thermal reservoirs. Thereunder are Cretaceous breccia and sandstone, among others, with a resistivity of more than 1000 Ω·m. Transversely, there were long-axial and plate-shaped low-resistance anomalies of beaded traps in the deep, which were presumed to be the fault reaction. Combining these data and the MT inversion results (2D + 3D), six faults were delineated, numbered F1–F6 (Figure 7):

1. F1: located in the northwest of the work area, northeast strike, northwest inclination, with a dip angle of about 60°–65° on the profile.
2. F2: located in the northwest of the work area, northeast strike, northwest inclination, with a dip angle of about 60°–65° on the profile.
3. F3: located in the west and middle of the work area, northeast strike, northwest inclination, with a dip angle of about 45°–60°on the profile.
4. F4: located in the middle of the work area, northeast strike, southeast inclination, with a dip angle of about 55°–70°on the profile.
5. F5: located in the southwest of the work area, northeast strike, southeast inclination, with a dip angle of about 50°–70° on the profile.

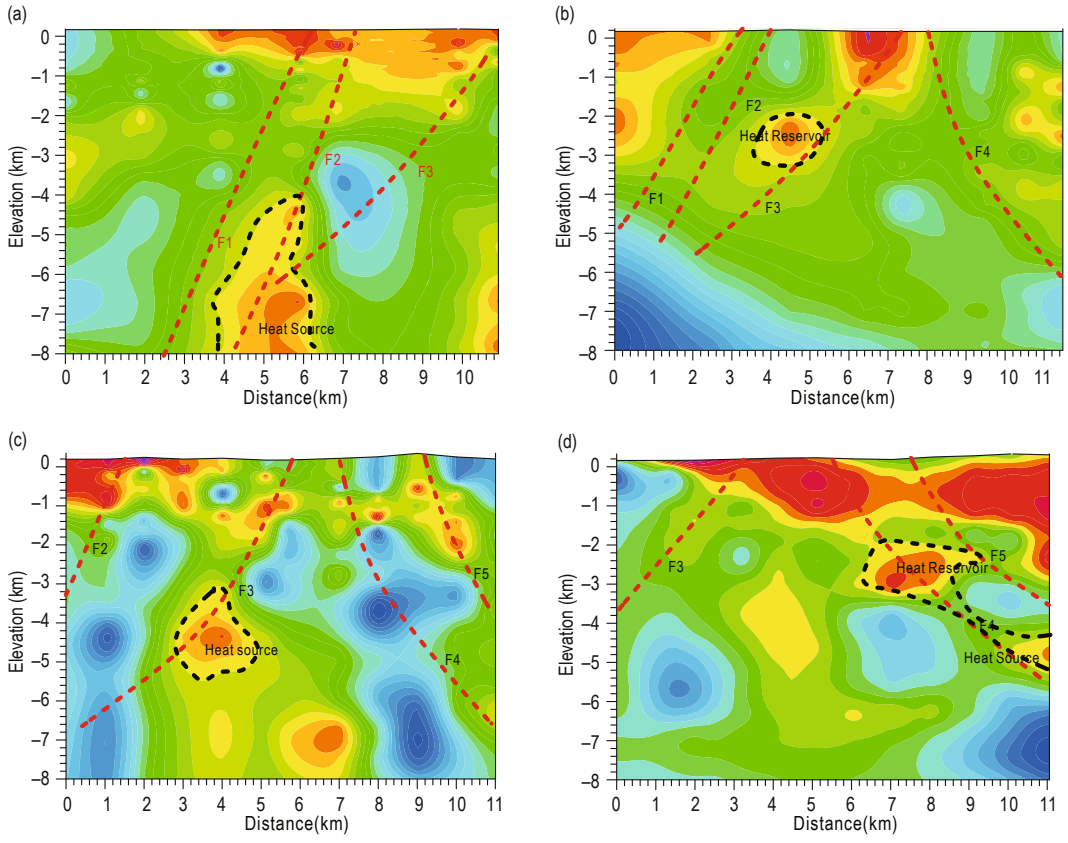

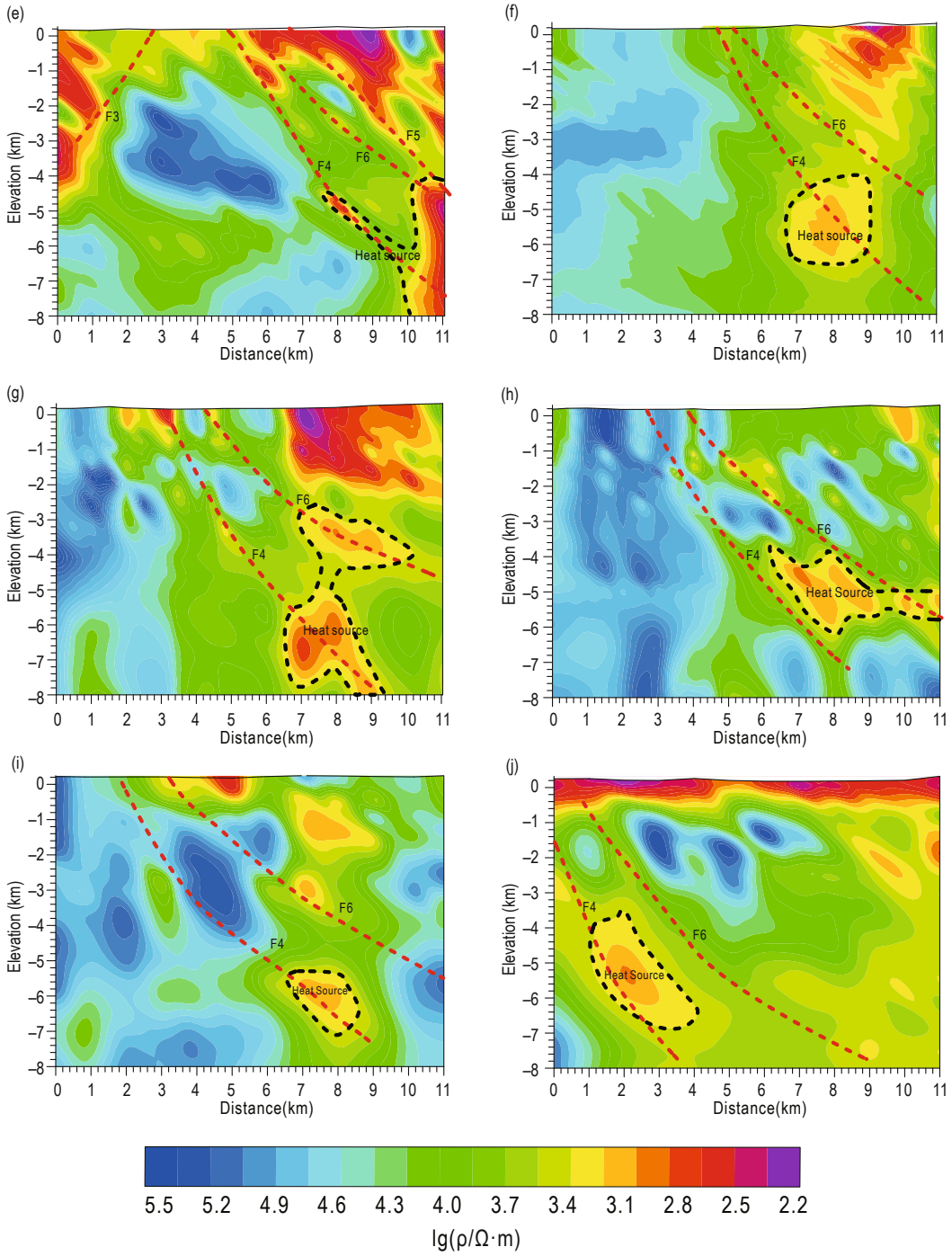

Figure 7. Resistivity profiles of the 10 survey lines.

6. F6: located in the southwest of the work area, northeast strike, southeast inclination, with an inclination angle of about 60°–70° on the profile.

According to the resistivity profile and the horizontal slices (Figure 8), the deep low-resistance anomaly moves upward through the channel with slightly higher resistivity, forming a relatively low-resistance layer and a low-resistance layer in the shallow part, corresponding to the thermal source, thermal conduction fracture, thermal reservoir, and caprock layer, respectively. This electrical structure is very similar to the convective geothermal resource structure model. More specifically, the inferred heat source and heat storage layer of F1 and F2 faults are located at a horizontal distance of 3.8–6.2 km to the L1 profile and an elevation of −3 km. The inferred heat source and heat storage layer of the F3 fault

are located within the 4 km depth range of the L2 and L3 profiles. The strip-shaped heat sources and heat storage layers develop at an elevation of 4 km in the F4 fault; the strike is consistent with the distribution direction of the fault, manifesting that the F4 fault has good heat conductivity and heat storage capability. Unfortunately, the heat source and heat storage layer are not delineated in the F5 and F6 fault areas.

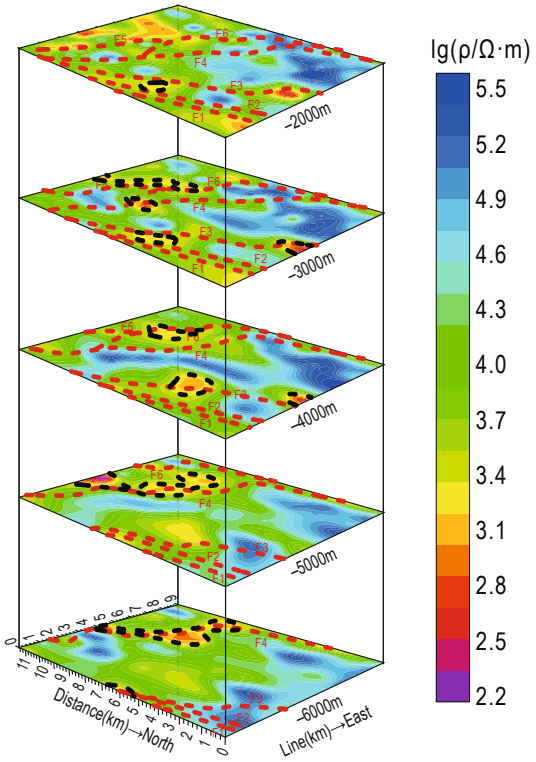

Figure 8. Horizontal slices at different depths.

On the basis of the above comprehensive analysis, the 3D thermal model was constructed as shown in Figure 9 (the blue parts indicate caprocks, whereas the red parts indicate geothermal sources and reservoirs). The Yishu fault zone is a geothermal anomaly distribution area controlled by faults, and the formation of geothermal energy is closely related to the long-term activity of deep and large faults. The main thermal reservoirs were dense sedimentary rock fractures, such as thin layers of purple-red fine sandstone in the conglomerate sandstones of the Wangshi Group and Dasheng Group in the Cretaceous. The Jiaonan uplift has been subjected to long-term strong weathering and denudation effects, and granite and Precambrian metamorphic rocks with high thermal conductivity and strong permeability were widely exposed, which facilitated underground heat flow conduction and atmospheric precipitation infiltration and contributed to the growth of the geothermal target layer. The type of thermal storage was a fractured belt type, mostly in a strip or elliptical shape on the plane. Its long axis direction was consistent with the direction of the thermal control fault, and the spatial form often presented an irregular mushroom shape.

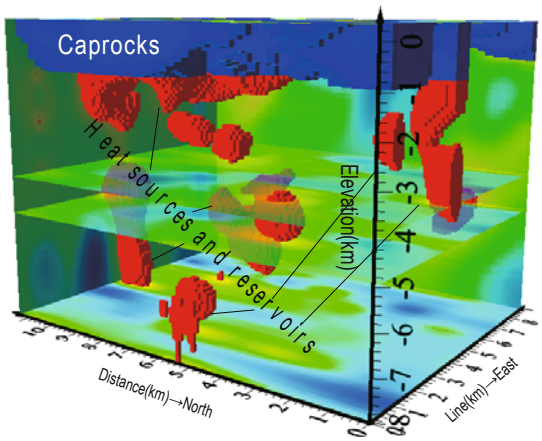

Figure 9. 3D geothermal model.

Conclusion

According to the results of the MT survey, the geothermal system was classified as a convective-type low-medium temperature geothermal system bordering on a high-temperature geothermal belt at the plate edge. The shallow part of the study area was a medium- and low-resistance layer, which was the caprock of the geothermal system, presumed to be composed of conglomerate, sandstone, shale, tuff, and andesite, among others. Below the caprock were thermal reservoirs with significantly increased resistivity, which were presumed to be intrusive rocks and metamorphic rocks. Transversely, there were long-axis and plate-shaped low-resistance anomalies of beaded traps in deep layers, which were probably the manifestation of fault anomalies. At the center or near the center of the structural uplift (or the core of the anticline), the shape of the geothermal anomalies, wide at the top and narrow at the bottom, was conducive to lateral migration, refraction, and redistribution of geothermal flow, leading to the convergence and concentration of geothermal flow from the outer edge of the uplift toward the center, finally forming a geothermal anomaly zone.

References

Agemar, T., 2022. Bottom hole temperature correction based on empirical correlation. Geothermics, **99**: 102296.

Berdichevsky, M.N. and Weaver, J.T., 1999. Marginal notes on magnetotellurics. Surveys in geophysics, **20**(3−4): 341−375.

Chen, H., Xie, X., Liu, E., Zhou, L. and Yan, L., 2021. Application of Infrared Remote Sensing and Magnetotelluric Technology in Geothermal Resource Exploration: A Case Study of the Wuerhe Area, Xinjiang. Remote Sensing, **13**(24): 4989.

Deng, Q. et al., 2021. Evaluation of favourable hot dry rock areas in the east of the Yishu fault zone in China. Australian Journal of Earth Sciences, **68**(2): 245−261.

Dmitriev, V.I. and Berdichevsky, M.N., 1979. The fundamental model of magnetotelluric sounding. Proceedings of the IEEE, **67**(7): 1034−1044.

Egbert, G.D., 1997. Robust multiple-station magnetotelluric data processing. Geophysical journal international, **130**(2): 475−496.

Egbert, G.D. and Kelbert, A., 2012. Computational recipes for electromagnetic inverse problems. Geophysical Journal International, **189**(1): 251−267.

Groom, R.W. and Bailey, R.C., 1989. Decomposition of magnetotelluric impedance tensors in the presence of local three-dimensional galvanic distortion. Journal of Geophysical Research: Solid Earth, **94**(B2): 1913−1925.

Kelbert, A., Meqbel, N., Egbert, G.D. and Tandon, K., 2014. ModEM: A modular system for inversion of electromagnetic geophysical data. Computers & Geosciences, **66**: 40−53.

Kun, Z. et al., 2020. Magnetotelluric evidence for the multi-microcontinental composition of eastern South China and its tectonic evolution. Scientific Reports, **10**(1).

Kunetz, G., 1972. PROCESSING AND INTERPRETATION OF MAGNETOTELLURIC SOUNDINGS. GEOPHYSICS, **37**(6): 1005−1021.

Lee, T.J., Han, N. and Song, Y., 2018. Magnetotelluric survey applied to geothermal exploration: An example at Seokmo Island, Korea. Exploration Geophysics, **41**(1): 61−68.

Li, X. et al., 2022. Magnetotelluric signatures of Neoproterozoic subduction, and subsequent lithospheric reactivation and thinning beneath central South China. Tectonophysics, **833**: 229365.

Liao, Y. et al., 2023a. A high geothermal setting in the Linyi geothermal field: Evidence from the lithospheric thermal structure. Energy Exploration & Exploitation, **41**(6): 1899−1918.

LIU Chunhua, WANG Wei and Zhengrun, W., 2018. Analysis of hydrothermal geothermal resources and its prospect of development and utilization in Shandong. Geological Survey of China, **2**(5): 51−53.

Liu, Y. et al., 2023. Characteristics of the stratigraphic reservoirs and caprocks of the geothermal resources in the Northwestern Shandong region. Energy Exploration & Exploitation, **41**(5): 1519−1538.

Maithya, J. and Fujimitsu, Y., 2019. Analysis and interpretation of magnetotelluric data in characterization of geothermal resource in Eburru geothermal field, Kenya. Geothermics, **81**: 12−31.

Mekkawi, M.M., Abd-El-Nabi, S.H., Farag, K.S. and Abd Elhamid, M.Y., 2022. Geothermal resources prospecting using magnetotelluric and magnetic methods at Al Ain AlSukhuna-Al Galala Albahariya area, Gulf of Suez, Egypt. Journal of African Earth Sciences, **190**: 104522.

Newman, G.A. and Alumbaugh, D.L., 2000. Three-dimensional magnetotelluric inversion using non-linear conjugate gradients. Geophysical journal international, **140**(2): 410−424.

Ogawa, Y. and Junge, A., 2002. On two-dimensional modeling of magnetotelluric field data. Surveys in Geophysics, **23**(2−3): 251−272.

Patro, P.K., 2017. Magnetotelluric Studies for Hydrocarbon and Geothermal Resources: Examples from the Asian Region. Surveys in Geophysics, **38**(5): 1005−1041.

Ritter, O., Junge, A. and Dawes, G., 1998. New equipment and processing for magnetotelluric remote reference observations. Geophysical Journal International, **132**(3): 535−548.

Rodi, W. and Mackie, R.L., 2001. Nonlinear conjugate gradients algorithm for 2-D magnetotelluric inversion. GEOPHYSICS, **66**(1): 174−187.

Siripunvaraporn, W., Egbert, G. and Uyeshima, M., 2005. Interpretation of two-dimensional magnetotelluric profile data with three-dimensional inversion: synthetic examples. Geophysical Journal International, **160**(3): 804−814.

Travassos, J.M. and Beamish, D., 1988. Magnetotelluric data processing--a case study. Geophysical Journal International, **93**(2): 377−391.

Vozoff, K., 1972. THE MAGNETOTELLURIC METHOD IN THE EXPLORATION OF SEDIMENTARY BASINS. GEOPHYSICS, **37**(1): 98−141.

Yang, H., Sun, Y. and Jiang, T., 2020. Study on geothermal genesis in Juxian area, Shandong Province. IOP Conference Series: Earth and Environmental Science, **558**(3): 032014.

Du Wenlong, Engineer, graduated from Shandong University of Science and Technology with a Bachelor's degree in Geophysics. He is currently an engineer in the Third Exploration Team of Shandong Coalfield Geological Bureau. He is engaged in electromagnetic data acquisition, processing and interpretation.

Zhou Xingyu, Senior engineer, graduated from China University of Geosciences (Wuhan) in Resource Exploration Engineering. He is currently a senior engineer in the Third Exploration Team of Shandong Coalfield Geological Bureau. His main interests are coal mine goaf exploration, geological disaster investigation and evaluation, geothermal investigation, and metal exploration.